Electronic Supplementary Information (ESI)

A multifunctional basic pH indicator probe for distinguishable detection of Co^{2+}, Cu^{2+} and Zn^{2+} with its utility in mitotracking and monitoring cytoplasmic viscosity in apoptotic cells

*E mail: singvp@yahoo.co.in

Pranjalee Yadav[a], Sarita Gond[a], Anusmita Shekher[b], Subash Chandra Gupta[b,c], Udai P. Singh[d], Vinod P. Singh[a*]

[a]Department of Chemistry, Institute of Science, Banaras Hindu University, Varanasi-221005 India

[b]Department of Biochemistry, Institute of Science, Banaras Hindu University, Varanasi 221005, India

[c]Department of Biochemistry, All India Institute of Medical Sciences, Guwahati, Assam, India

[d]Department of Chemistry, Indian Institute of Technology Roorkee, Roorkee 247667, India

Table of Contents

	Experimental	S3-S5
Fig. S1	IR spectrum of HNH	S6
Fig. S2	^{1}H NMR spectrum of HNH	S7
Fig. S3, S4	^{13}C NMR spectrum of HNH and IR spectrum of HMN	S8
Fig. S5, S6	^{1}H NMR and ^{13}C NMR spectrum of HMN	S9
Fig. S7	Mass spectrum of HMN	S10
Table S1	Crystallographic data for HMN	S11
Table S2, S3	Selected bond length (Å) and angle (º) for HMN, and H-bonding in HMN [Å and °]	S12, S13
Fig. S8, S9	Intra and Inter-molecular H-bonding in HMN, and Hirshfeld surface analysis and 2D fingerprint plot of HMN	S14
Fig. S10, S11	UV-Vis spectra of HMN (20 μM) in DMF:Water (9:1 v/v, HEPES 10 mM) at variable pH, and fluorescence spectra of HMN (5 μM, λ_{ex} = 410 nm) in DMF:water binary mixture of varied water fraction (f_{water})	S15
Fig. S12, S13	Job's plot between HMN with (a) Co^{2+}, (b) Cu^{2+} and (c) Zn^{2+}, and limit of detection (LOD) curve plot and Benesi–Hildebrand plot of HMN assuming 1:1 binding stoichiometry with Cu^{2+}	S16
Fig. S14, S15	LOD curve plots and Benesi–Hildebrand plots of HMN with Cu^{2+} and Co^{2+}, and fluorescence bar diagram of HMN (20 μM) with various metal ions	S17
Fig. S16, S17	Competitive selectivity of HMN (5μM) towards Zn^{2+} in presence of other metal ions, and Limit of detection (LOD) curve plot and Benesi-Hildebrand plot of HMN assuming 1:1 binding stoichiometry with Zn^{2+}	S18
Fig. S18	^{1}H NMR titration of HMN upon addition of Zn^{2+} (0-1 equiv.) in DMSO–d_6	S19
Fig. S19, S20	Mass spectrum of HMN-Zn^{2+} complex, and IR spectrum of HMN, HMN-Zn^{2+}, HMN-Cu^{2+} and HMN-Co^{2+} complexes	S20
Table S4, Fig. S21	Comparison of experimental and theoretical vibrational frequencies of HMN and HMN-Zn^{2+}, and diagram displaying electronic transitions associated with HMN and HMN-Zn^{2+}	S21
Table S5	TD-DFT calculations for UV–visible transitions in HMN and HMN-Zn^{2+} complex with their assignments	S22
Fig. S22, S23	Normalized absorption and emission spectra of HMN, and viability of cells examination by MTT assay after treatment of SiHa cells with indicated concentrations of HMN for 24 hrs at neutral pH	S23
Table S6	Comparison of HMN with past reported probes	S24
	References	S25

1. Experimental

***Synthesis of (Z)-1-(hydrazonomethyl)napthalen-2-ol* (HNH)**

An excess of hydrazine hydrate (100 mM, 5 mL) was placed in a round bottomed flask over magnetic stirrer. To this, an ethanolic solution of 2-hydroxy-1-naphthaldehyde (10 mM, 1.72 g) was added drop wise with continuous stirring. After stirring for 4 hours, the filtrate was poured into cold water which led to immediate precipitation. The precipitate was filtered and dried in a desiccator over anhydrous calcium chloride.

Analytical data: Pale yellow solid, Yield 80%. M.P. 130 °C, *Anal. Calc.* for $C_{11}H_{10}N_2O$ (186): IR (KBr, cm^{-1}): ν(O-H) 3415, ν(N-H) 3293, ν(C=N) 1618, ν(N-N) 949. ^{1}H NMR (δ ppm) (DMSO-d_6): 12.83 (s, 1H, OH), 8.87 (s, 1H, =CH), 8.1−7.1 (6H, aromatic protons), 7.0 (s, 2H, NH_2). ^{13}C NMR (δ ppm) (DMSO-d_6): 156.0 (C-OH); 139.7 (C=N); 130.8–109.5 (aromatic carbons).

General procedures

Millipore water was utilized in the preparation of stock solutions of metal chlorides (1×10^{-2} M). A stock solution of **HMN** (1×10^{-2} M) was prepared in DMF and then diluted with aqueous HEPES buffer (pH 7) to acquire the solution concentration of 1×10^{-2} M (DMF:Water 9:1, v/v, HEPES buffer, pH 7) for different experiments. The pH of various solutions were maintained with the help of pH meter instrument. For the titrations, **HMN** solution (1×10^{-2} M) was titrated with incremental concentration of the solutions of metal ions (1×10^{-3} M). All the measurements were carried out at room temperature in DMF:Water (9:1, v/v, HEPES buffer, pH 7). The excitation wavelength of 410 nm was set for all the fluorescence experiments. The binding ratio between **HMN** and metal ions were computed from Job's plot, and binding constants (K_a) of **HMN** for Co^{2+} and Cu^{2+} were calculated with the help of Benesi–Hildebrand

equation (1).[1] Binding constant of **HMN** for Zn^{2+} was calculated by linear fitting of UV-vis titration data in the equation (2).

$$1/(A-A_0) = 1/(K_a(A_{max} - A_0)[Metal]) + 1/(A_{max} - A_0) \quad (1)$$

Where, A and A_0 are the absorbance of **HMN** with and without metal ions (Co^{2+} and Cu^{2+}), respectively, A_{max} is the maximum absorbance of **HMN** with excess of metal ions, and $[M^{2+}]$ is the metal ions added.

$$I_0/I - I_0 = (a/b\text{-}a)(1/K_a[Metal] + 1) \quad (2)$$

where, I and I_0 represent the fluorescence intensities of **HMN** at 500 nm in the presence and absence of Zn^{2+} ; a, b are constants; [Metal] is the Zn^{2+} concentration.

The Detection limit (LOD) for **HMN** was computed with the help of equation (3). The slope was acquired from a linear fitting plot of absorbance/fluorescence ratio versus concentration of metal ions added.[2]

$$LOD = 3\sigma/slope \quad (3)$$

Computational details

Computational calculations for **HMN** and **HMN**-Zn^{2+} complex were executed on Gaussian-09 program using 6-311G (d,p) basis set and RB3LYP method. DFT optimized structures were confirmed to be minima on potential energy surface. TDDFT calculations were carried out at the same RB3LYP level to correlate the electronic transitions.[3]

X-ray structure analysis

The X-ray data of **HMN** was collected and analyzed on Bruker Smart Apex-II CCD diffractometer, using graphite monochromated Mo-Kα radiation ($\lambda = 0.71070$ Å) at 296 K. Structure solving, data output and refinement were executed on SHELXTL program.[4] All the

non-hydrogen atoms were analyzed anisotropically and final images were created with the help of ORTEP program.

Hirshfeld surface analysis

Crystal Explorer 3.1 software was used to generate the molecular Hirshfeld surface maps and 2D fingerprint plots. The normalized contact distance (d_{norm}) can be expressed as

$$d_{norm} = \frac{\left(d_i - r_i^{vdW}\right)}{r_i^{vdW}} + \frac{\left(d_e - r_e^{vdW}\right)}{r_e^{vdW}}$$

(4)

Where, r_i^{vdW} and r_e^{vdW} are the van-der-Waals radii. d_{norm} represents the red-white-blue color scheme surface. The bright red spots represent shorter contacts, the white color area represents short contact interactions within the van der Waals distance and the blue color regions represent no close contacts. The normalized contact distance (d_{norm}) based on both d_e and d_i (where d_e is the distance from a point on the surface to the nearest nucleus outside the surface and d_i is the distance from a point on the surface to the nearest nucleus inside the surface) and the vdW radii facilitate the recognition of the area of importance to intermolecular interactions.[5] The combination of *d*e and *d*i in the form of a 2D fingerprint plot[6] provides a summary of intermolecular contacts in the crystal.

Fluorescence quantum yield measurements

Quantum yield was calculated by using following equation:

$$Q = Q_r(I/I_r) \times (OD_r/OD) \times (n^2/n_r^2) \quad (4)$$

Where, **Q** and **I** are the fluorescence quantum yield and integrated fluorescence intensity, respectively. **n** and **OD** are the refractive index of solvent and optical density (absorption),

respectively. The subscript **r** infers to the reference quinine sulphate with quantum yield value of 0.54 in 0.1 M H_2SO_4.[7]

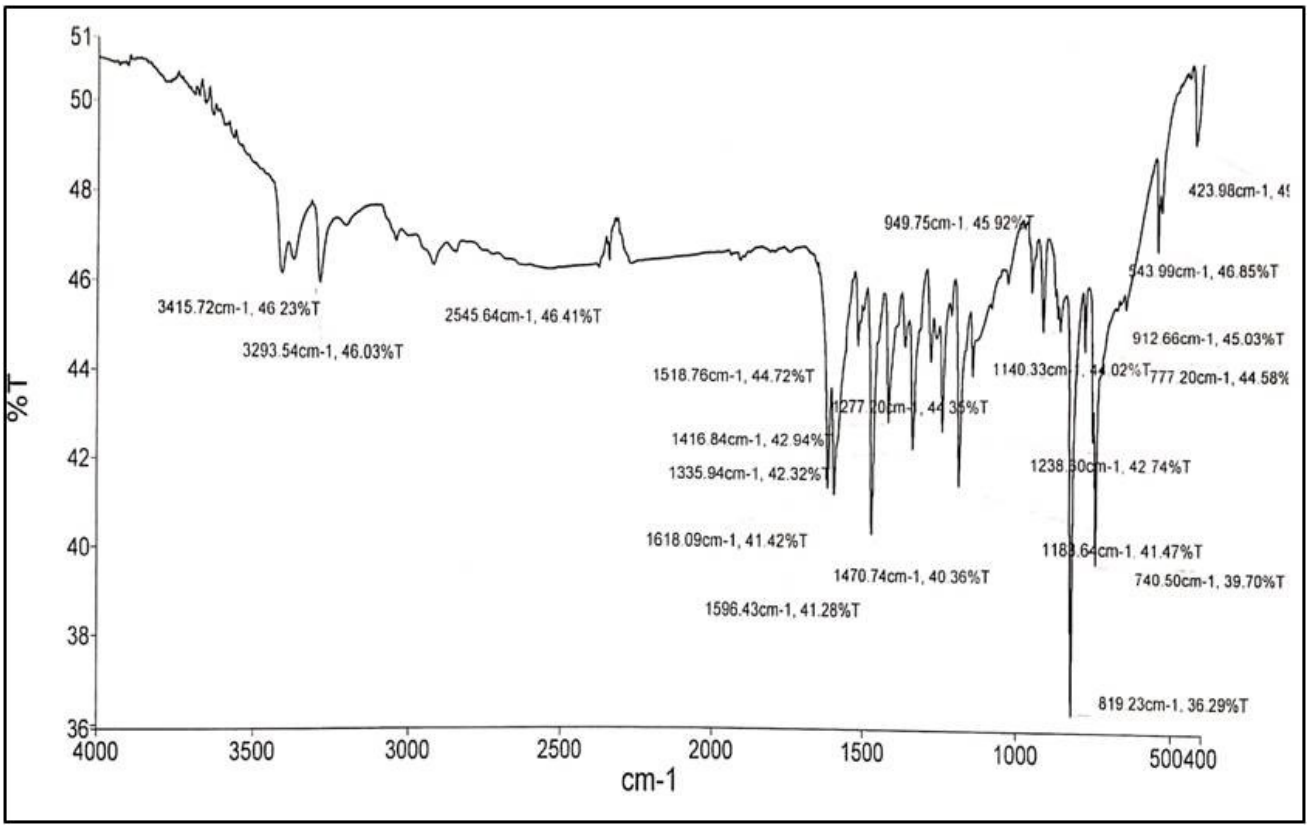

Fig. S1 IR spectrum of HNH

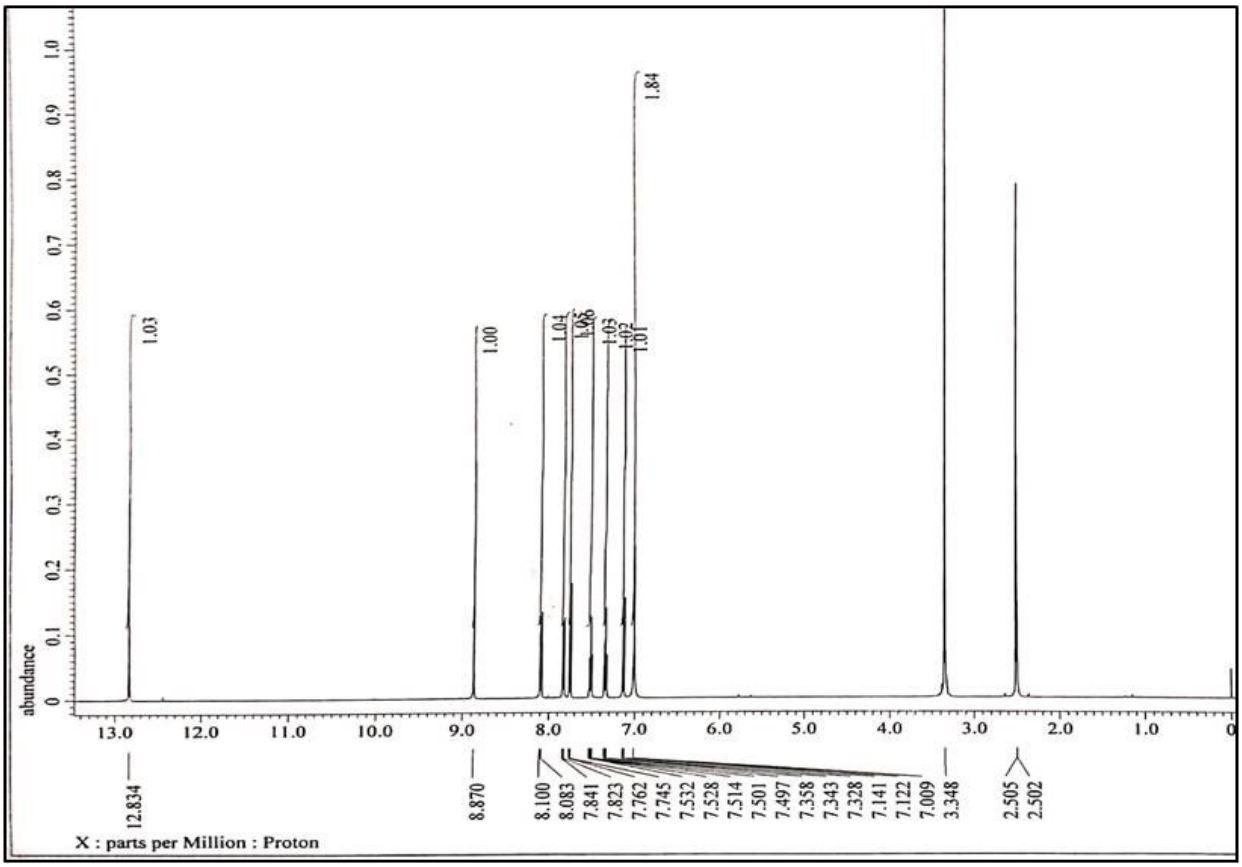

Fig. S2 ^{1}H NMR spectrum of HNH

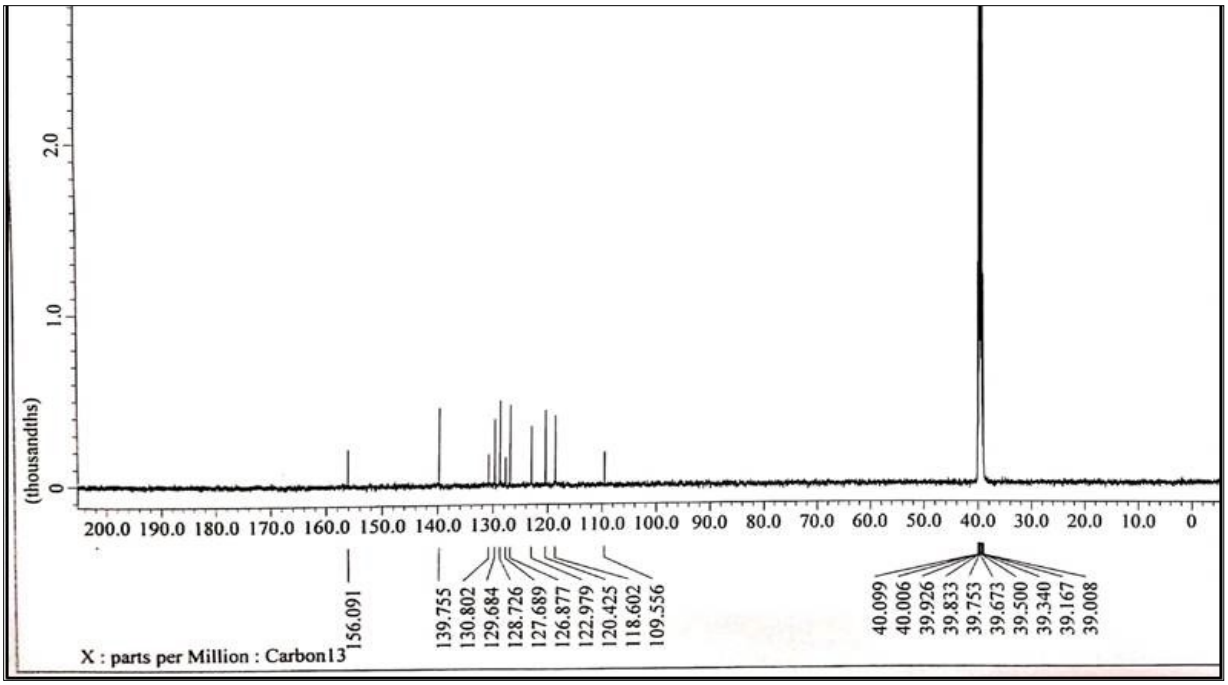

Fig. S3 ^{13}C NMR spectrum of HNH

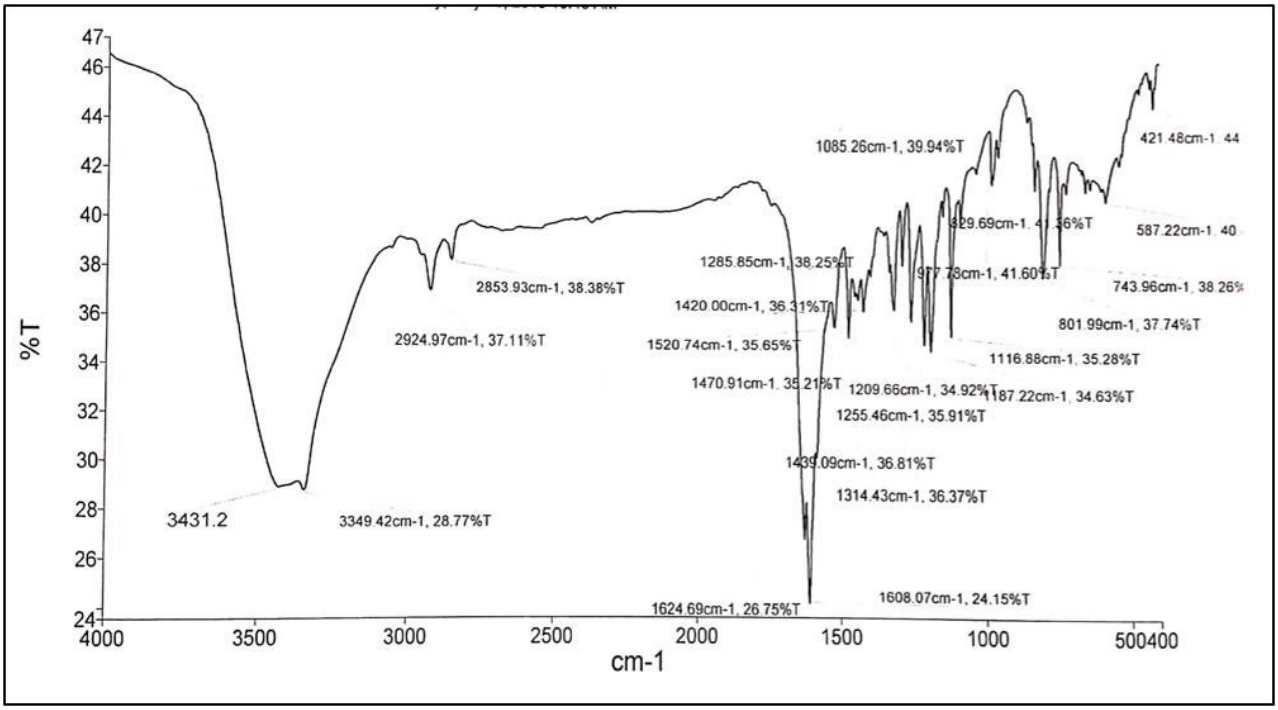

Fig. S4 IR spectrum of **HMN**

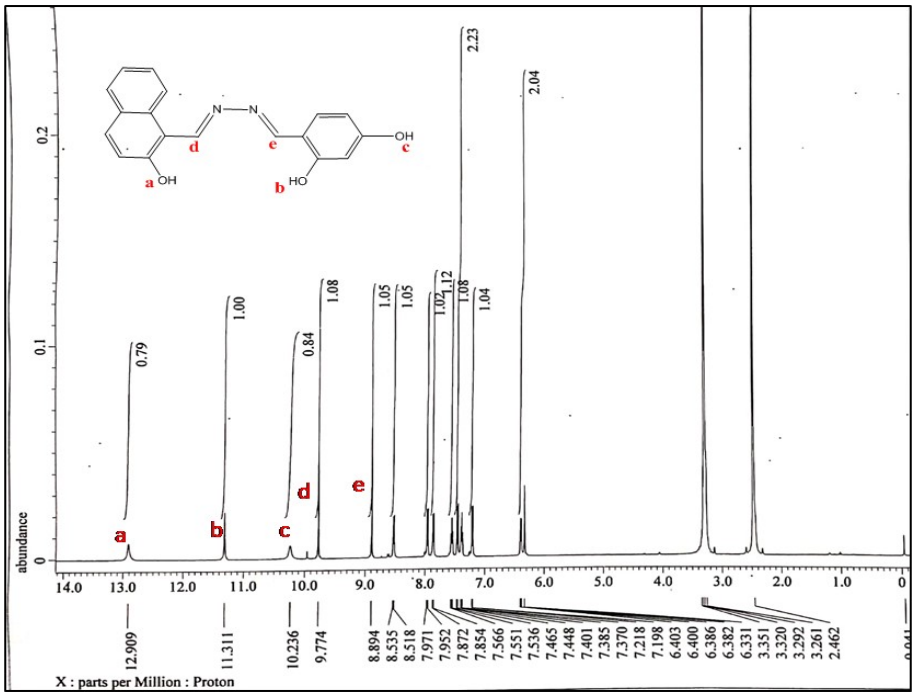

Fig. S5 ^{1}H NMR spectrum of **HMN**

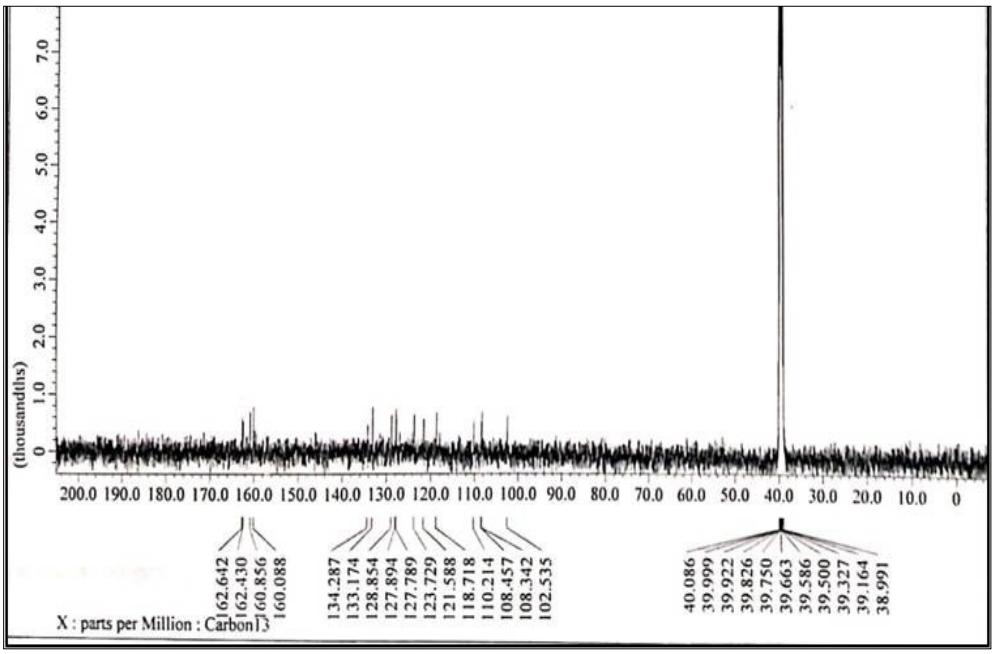

Fig. S6 ^{13}C NMR spectrum of **HMN**

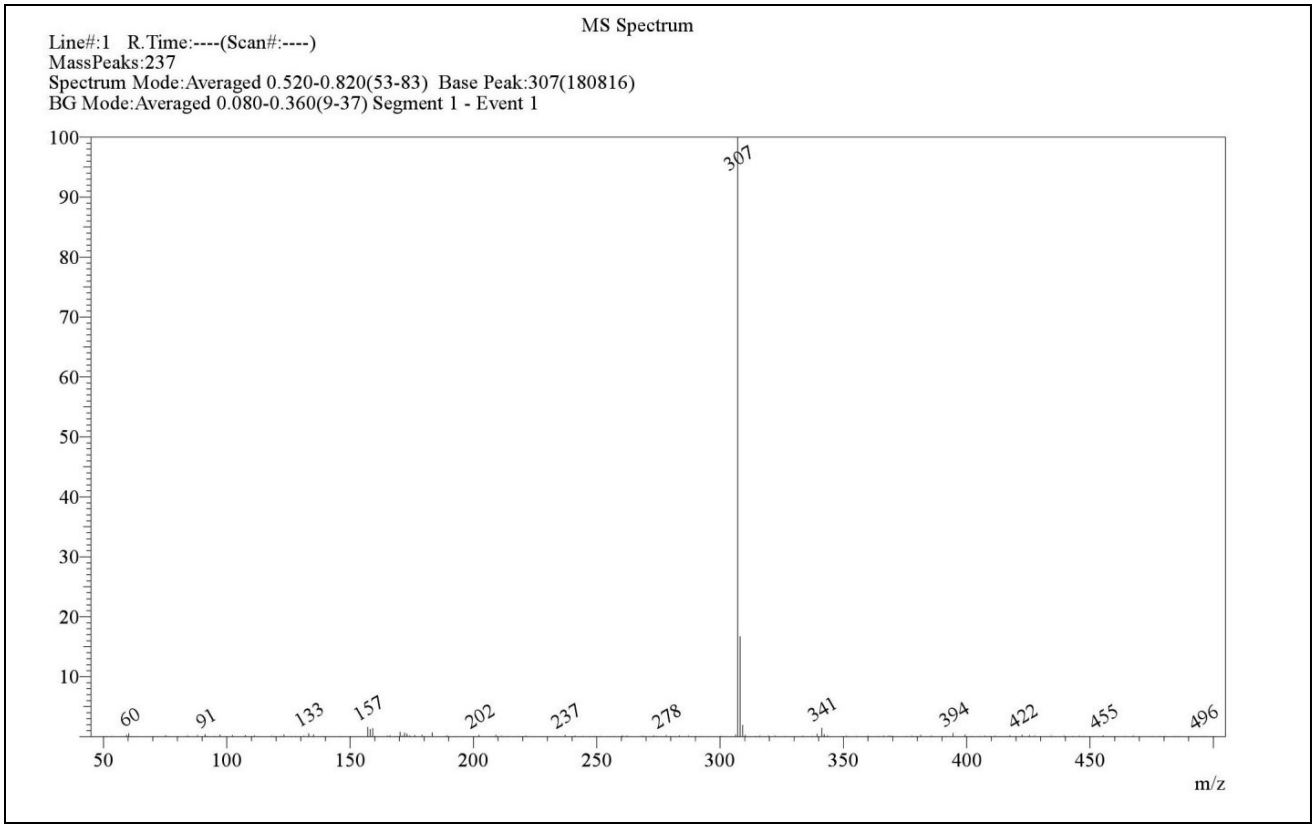

Fig. S7 Mass spectrum of **HMN**

Table S1: Crystallographic data for **HMN**

Empirical formula	$C_{18}H_{14}N_2O_3$
Formula weight	306
Temperature (K)	296(2)K
Wavelength (Å)	0.71073 Å
Crystal system	Monoclinic
Space group	C c
a (Å)	11.2643(8)
b (Å)	12.9129(9)
c (Å)	9.9050(7)
α (º)	90°
β (º)	92.136(2)
γ (º)	90°
Volume ($Å^3$)	1439.73(18)
Z	4
Density (Mg/m^3)	1.413
μ (mm^{-1})	0.098
F(000)	640
Crystal size (mm)	$0.23\times0.17\times0.12$ mm^3
θ range for data collection (º)	3.206 to 28.278°
No. of reflections collected	18066
No. of independent reflections (R_{int})	3404 [R(int) = 0.0310])
Number of data/restraints/parameters	3404/2/220
Goodness-of-fit on F^2	1.075
R_1, wR_2 [a,b][(I>2σ(I))]	0.0508, 0.1066
R_1, wR_2[a,b] (all data)	0.0751, 0.1232
Largest difference in peak and hole ($e.Å^{-3}$)	0.179 and -0.186

[a] $R_1 = \Sigma||F_o| - |Fc||\Sigma|F_o|$. [b] $R_2 = [\Sigma w(|F^2_o| - |F^2_c|)^2/\Sigma w|F^2_o|^2]^{1/2}$

Table S2: Selected bond length (Å) and angle (º) for **HMN** (corresponding to Fig. 1a)

Bond lengths			
O(1)-C(1)	1.355(5)	C(6)-C(7)	1.391(6)
O(1)-H(1O)	0.93(6)	C(6)-H(6A)	0.9300
O(2)-C(14)	1.365(5)	C(7)-C(8)	1.373(6)
O(2)-H(2O)	0.89(7)	C(7)-H(7A)	0.9300
O(3)-C(16)	1.369(4)	C(8)-C(9)	1.414(5)
O(3)-H(3O)	0.99(8)	C(8)-H(8A)	0.9300
N(1)-C(11)	1.291(5)	C(9)-C(10)	1.436(5)
N(1)-N(2)	1.403(4)	C(10)-C(11)	1.436(5)
N(2)-C(12)	1.283(5)	C(11)-H(11A)	0.9300
C(1)-C(10)	1.393(5)	C(12)-C(13)	1.442(5)
C(1)-C(2)	1.410(5)	C(12)-H(12A)	0.9300
C(2)-C(3)	1.355(6)	C(13)-C(18)	1.398(5)
C(2)-H(2A)	0.9300	C(13)-C(14)	1.401(5)
C(3)-C(4)	1.416(6)	C(14)-C(15)	1.370(6)
C(3)-H(3A)	0.9300	C(15)-C(16)	1.379(6)
C(4)-C(5)	1.406(5)	C(15)-H(15A)	0.9300
C(4)-C(9)	1.417(5)	C(16)-C(17)	1.394(5)
C(5)-C(6)	1.364(6)	C(17)-C(18)	1.376(5)
C(5)-H(5A)	0.9300	C(17)-H(17A) C(18)-H(18A)	0.9300 0.9300
Bond Angles			
C(1)-O(1)-H(1O)	105(4)	C(8)-C(9)-C(10)	123.4(4)
C(14)-O(2)-H(2O)	113(5)	C(4)-C(9)-C(10)	119.5(3)
C(16)-O(3)-H(3O)	110(6)	C(1)-C(10)-C(11)	120.1(4)
C(11)-N(1)-N(2)	114.1(3)	C(1)-C(10)-C(9)	118.5(3)
C(12)-N(2)-N(1)	113.9(3)	C(11)-C(10)-C(9)	121.4(3)
O(1)-C(1)-C(10)	122.9(3)	N(1)-C(11)-C(10)	122.3(3)
O(1)-C(1)-C(2)	115.8(3)	N(1)-C(11)-H(11A)	118.8

C(10)-C(1)-C(2)	121.3(4)	C(10)-C(11)-H(11A)	118.8
C(3)-C(2)-C(1)	120.2(4)	N(2)-C(12)-C(13)	121.3(4)
C(3)-C(2)-H(2A)	119.9	N(2)-C(12)-H(12A)	119.3
C(1)-C(2)-H(2A)	119.9	C(13)-C(12)-H(12A)	119.3
C(2)-C(3)-C(4)	121.2(4)	C(18)-C(13)-C(14)	117.2(3)
C(2)-C(3)-H(3A)	119.4	C(18)-C(13)-C(12)	120.1(3)
C(4)-C(3)-H(3A)	119.4	C(14)-C(13)-C(12)	122.7(3)
C(5)-C(4)-C(3)	120.7(4)	O(2)-C(14)-C(15)	118.2(3)
C(5)-C(4)-C(9)	120.1(4)	O(2)-C(14)-C(13)	120.3(3)
C(3)-C(4)-C(9)	119.3(3)	C(15)-C(14)-C(13)	121.5(3)
C(6)-C(5)-C(4)	121.0(4)	C(14)-C(15)-C(16)	119.7(3)
C(6)-C(5)-H(5A)	119.5	C(14)-C(15)-H(15A)	120.1
C(4)-C(5)-H(5A)	119.5	C(16)-C(15)-H(15A)	120.1
C(5)-C(6)-C(7)	119.8(4)	O(3)-C(16)-C(15)	122.3(3)
C(5)-C(6)-H(6A)	120.1	O(3)-C(16)-C(17)	117.0(3)
C(7)-C(6)-H(6A)	120.1	C(15)-C(16)-C(17)	120.7(3)
C(8)-C(7)-C(6)	120.5(4)	C(18)-C(17)-C(16)	118.7(3)
C(8)-C(7)-H(7A)	119.7	C(18)-C(17)-H(17A)	120.7
C(6)-C(7)-H(7A)	119.7	C(16)-C(17)-H(17A)	120.7
C(7)-C(8)-C(9)	121.5(4)	C(17)-C(18)-C(13)	122.0(3)
C(7)-C(8)-H(8A)	119.3	C(17)-C(18)-H(18A)	119.0
C(9)-C(8)-H(8A)	119.3	C(13)-C(18)-H(18A)	119.0
C(8)-C(9)-C(4)	117.1(3)		

Table S3. Hydrogen bonds for **HMN** [Å and °]

D-H...A	d(D-H)	d(H...A)	d(D...A)	<(DHA)
O(1)-H(1O)...N(1)	0.93(6)	1.73(6)	2.576(5)	150(5)
O(2)-H(2O)...N(2)	0.89(7)	1.83(7)	2.596(5)	142(6)
O(3)-H(3O)...O(2)#1	0.99(8)	1.86(9)	2.824(4)	166(8)

Symmetry transformations used to generate equivalent atoms:

#1 x,-y+1,z-1/2

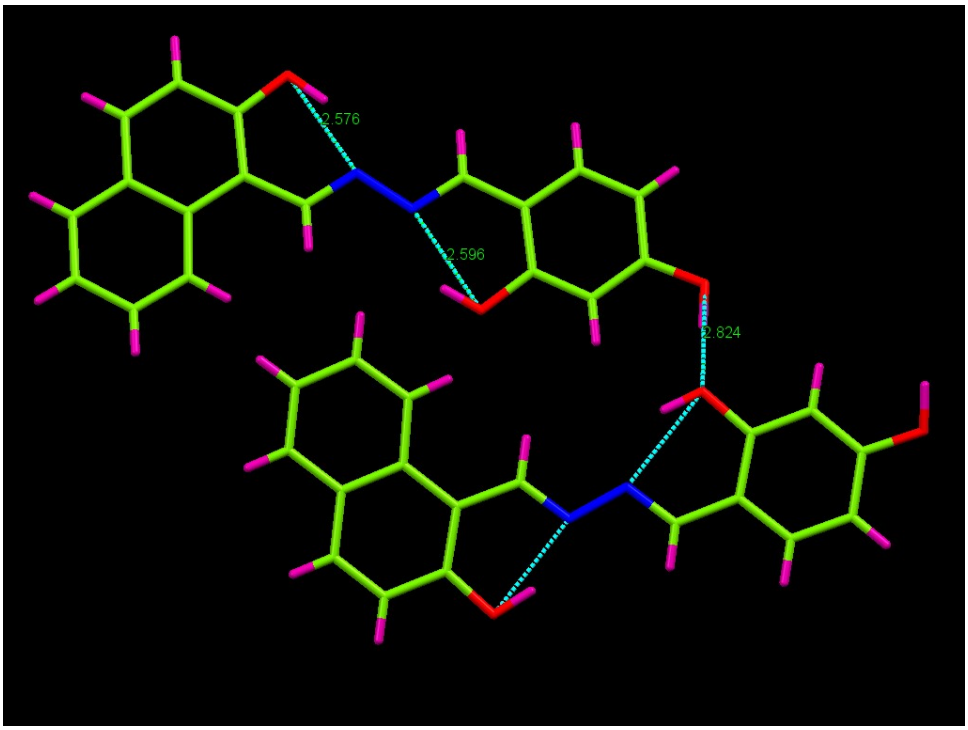

Fig. S8 Intra and Inter-molecular H-bonding in **HMN**

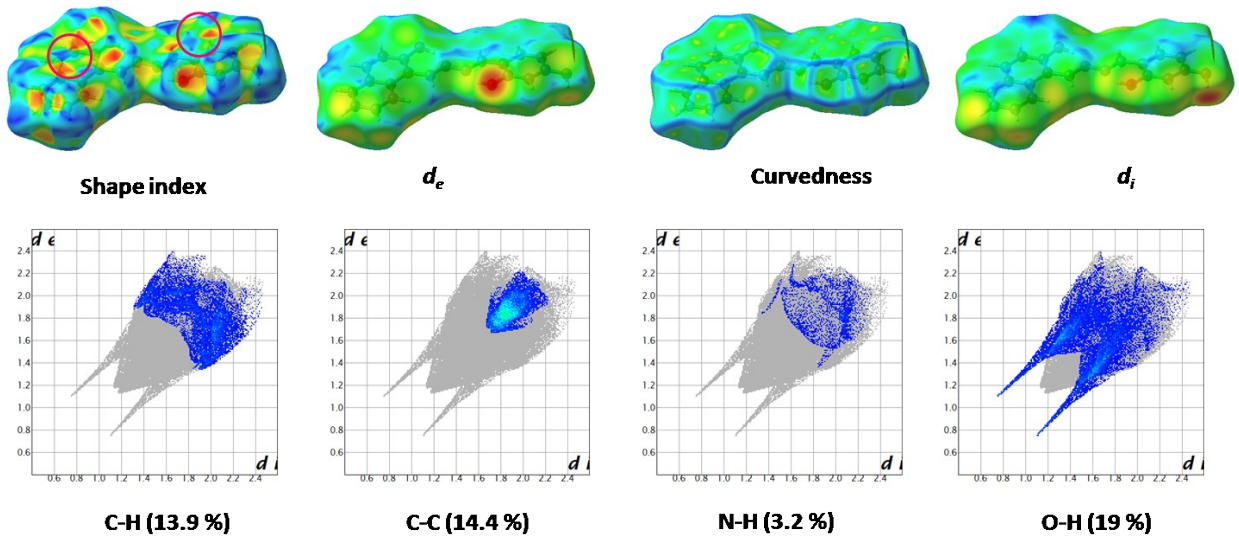

Fig. S9 (a) Hirshfeld surface analysis mapped over Shape index, d_e, curvedness and d_i (b) 2D fingerprint plot of **HMN** displaying percentage of C-H, C-C, N-H and O-H interactions

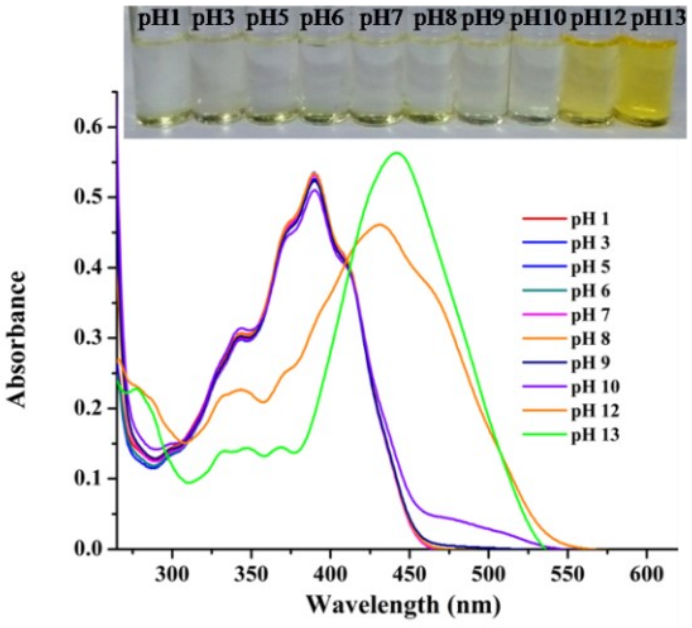

Fig. S10 UV-Vis spectra of **HMN** (20 μM) in DMF: Water (9:1 v/v, HEPES 10 mM) at variable pH

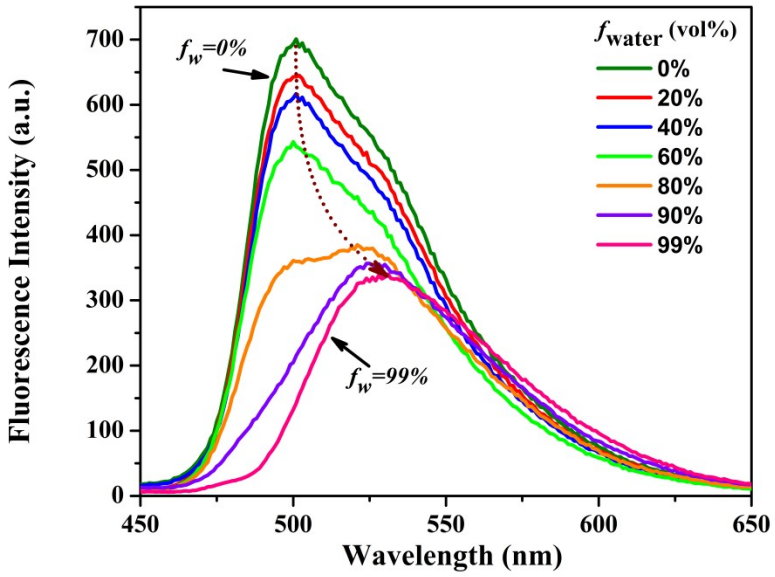

Fig. S11 Fluorescence spectra of **HMN** (5 μM, λ_{ex} = 410 nm) in DMF:water binary mixture of varied water fraction (f_{water})

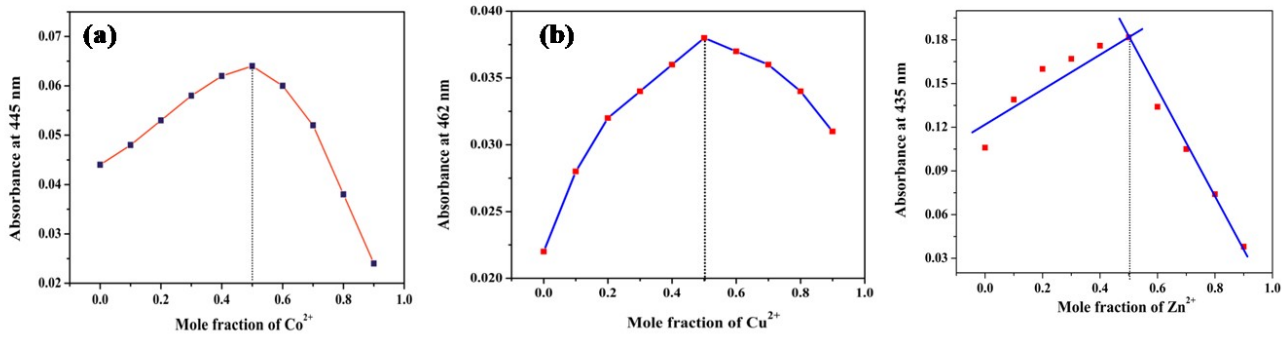

Fig. S12 Job's plot for determination of stoichiometry between **HMN** with (a) Co^{2+} and (b) Cu^{2+} (c) Zn^{2+}

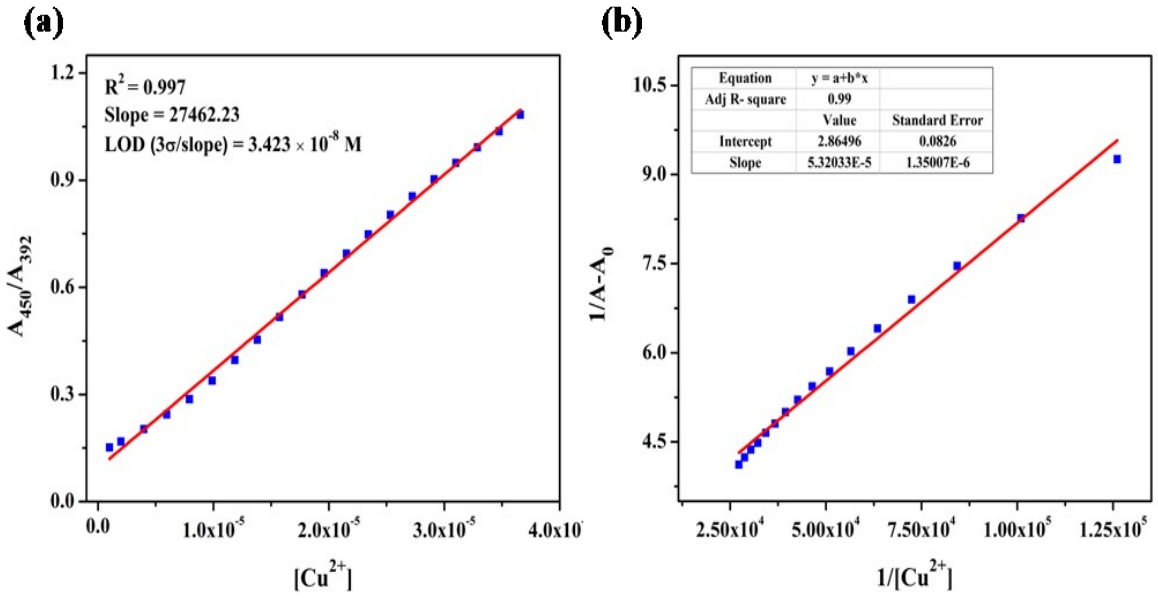

Fig. S13 (a) Limit of detection (LOD) curve plot (b) Benesi–Hildebrand plot of **HMN** (absorbance at 450 nm) assuming 1:1 binding stoichiometry with Cu^{2+}. Goodness of fit is denoted by R^2.

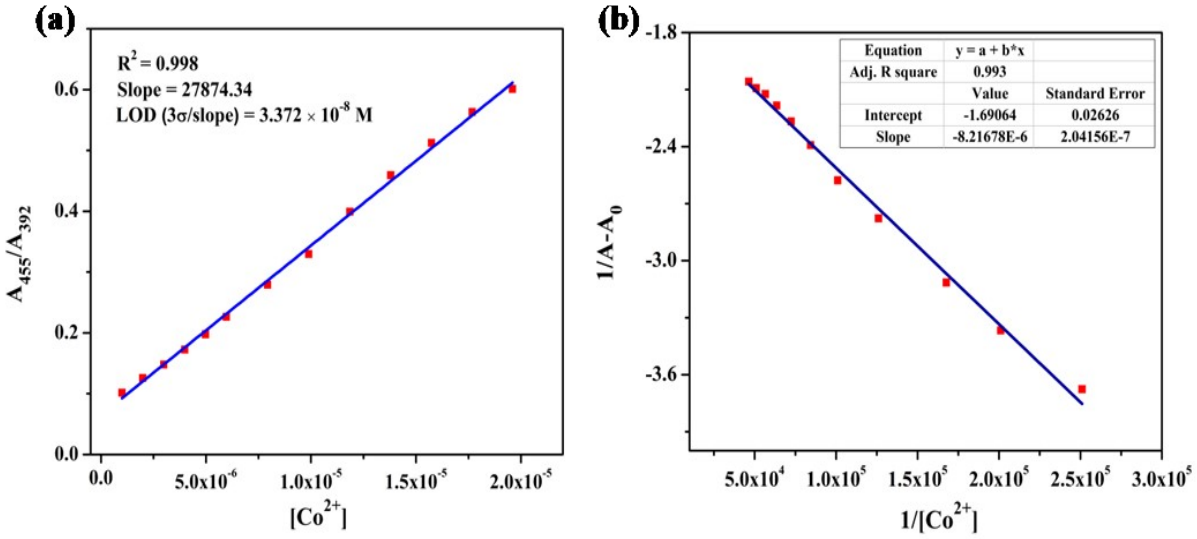

Fig. S14 (a) Limit of detection (LOD) curve plot (b) Benesi–Hildebrand plot of **HMN** (absorbance at 392 nm) assuming 1:1 binding stoichiometry with Co^{2+}. Goodness of fit is denoted by R^2.

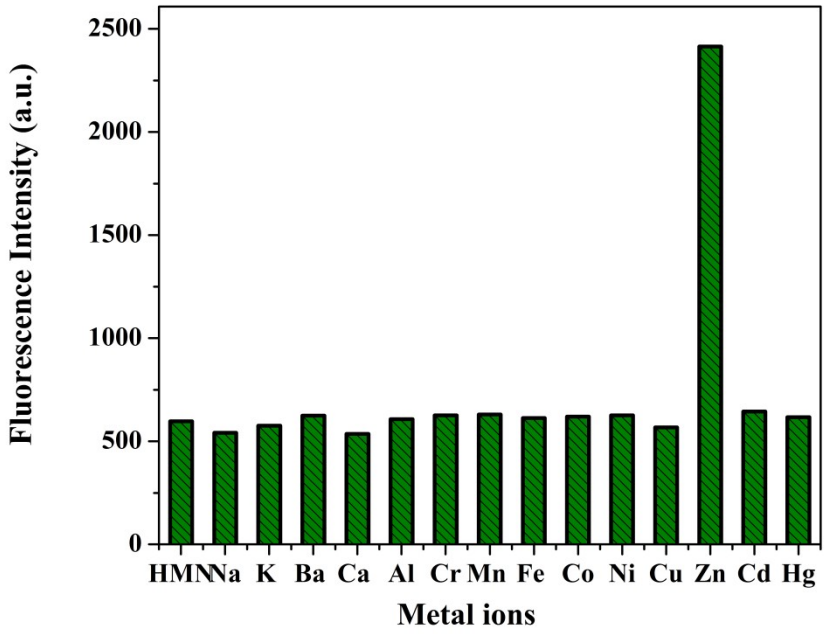

Fig. S15 Fluorescence bar diagram of **HMN** (20 μM) with various metal ions (λ_{em} = 508 nm, λex = 400 nm).

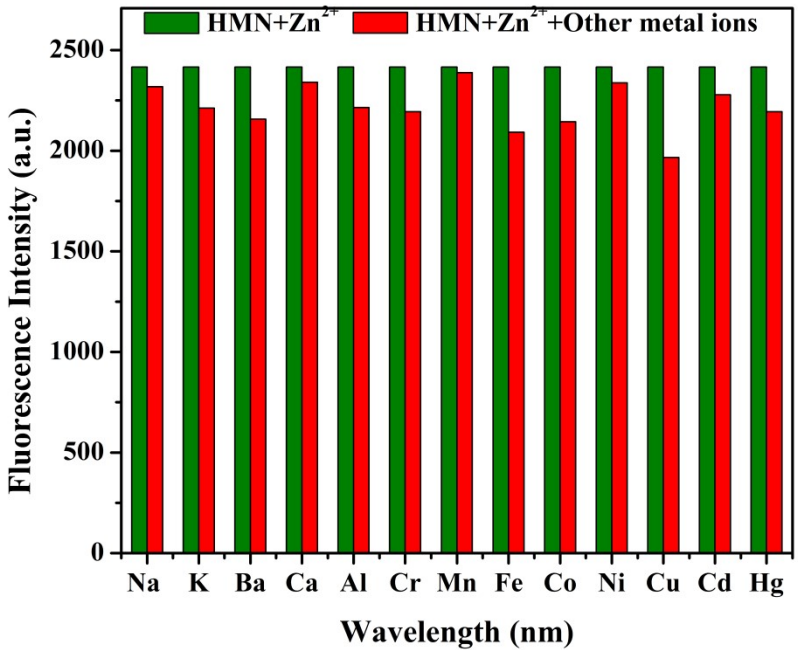

Fig. S16 Competitive selectivity of **HMN** (5μM) towards Zn^{2+} in presence of other metal ions (λ_{em} = 500 nm, λex = 400 nm).

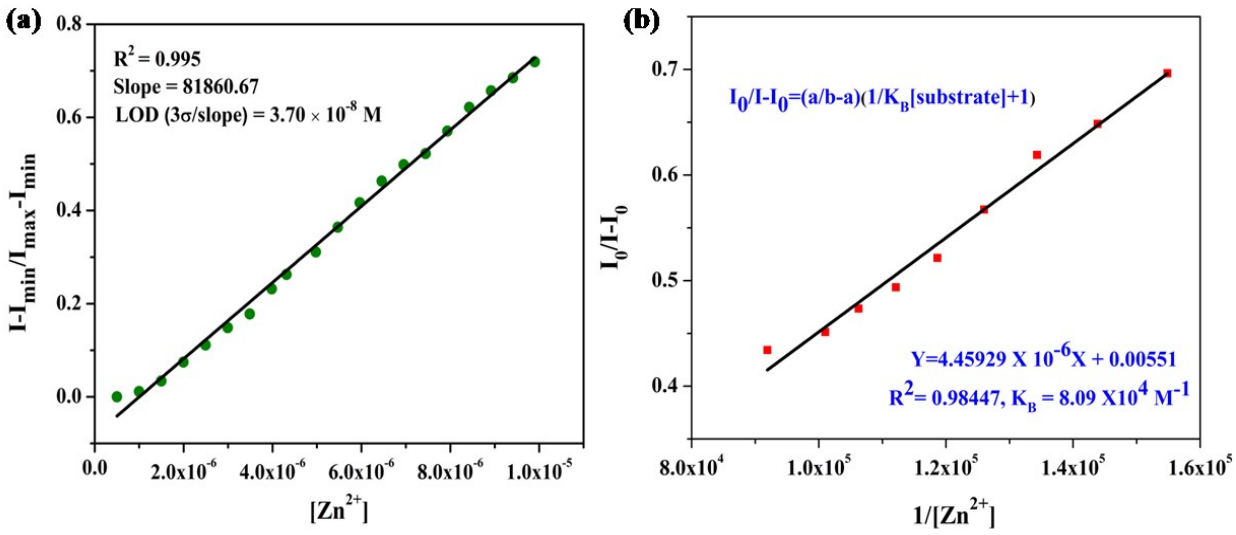

Fig. S17 (a) Limit of detection (LOD) curve plot. (b) Benesi-Hildebrand plot of **HMN** assuming 1:1 binding stoichiometry with Zn^{2+}.

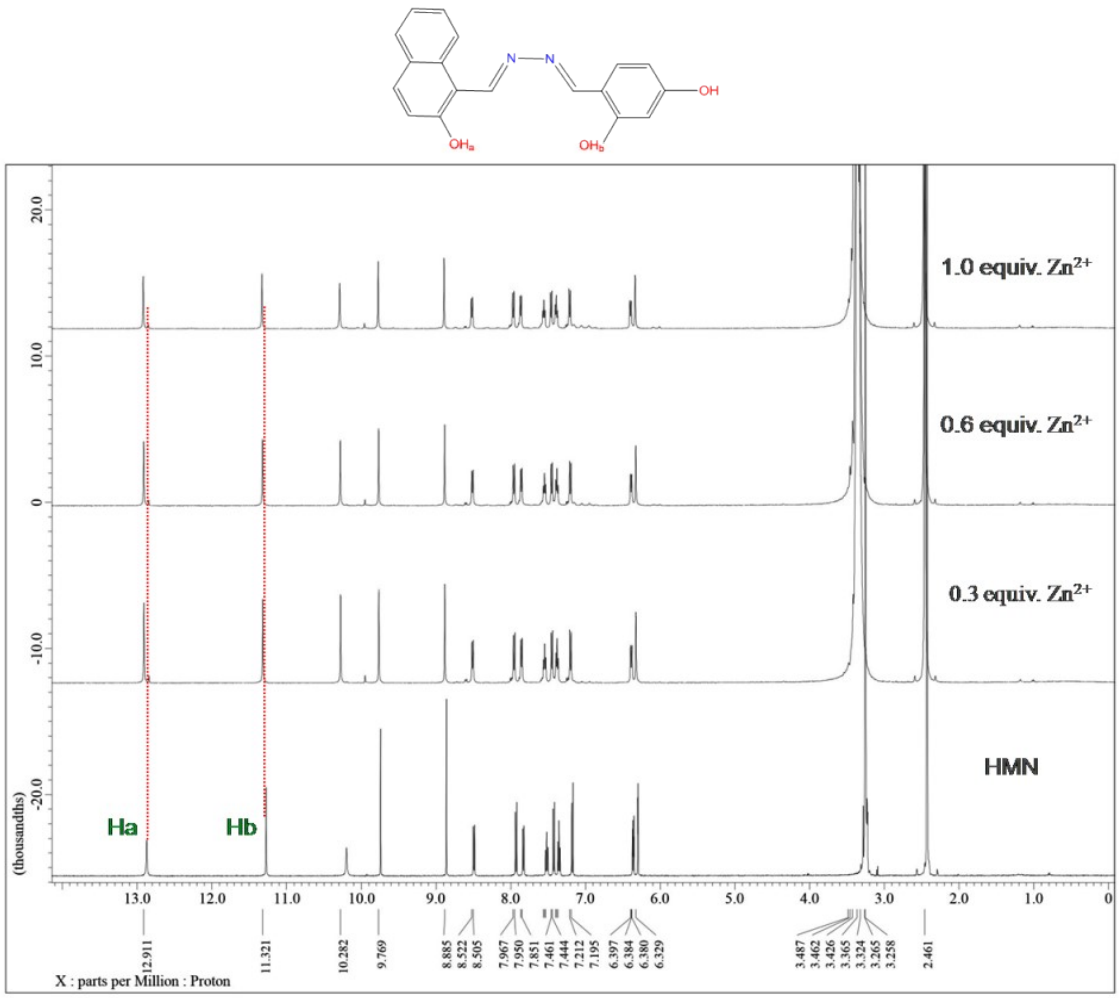

Fig. S18. ^{1}H NMR titration of **HMN** upon addition of Zn^{2+} (0-1 equiv.) in DMSO–d_6

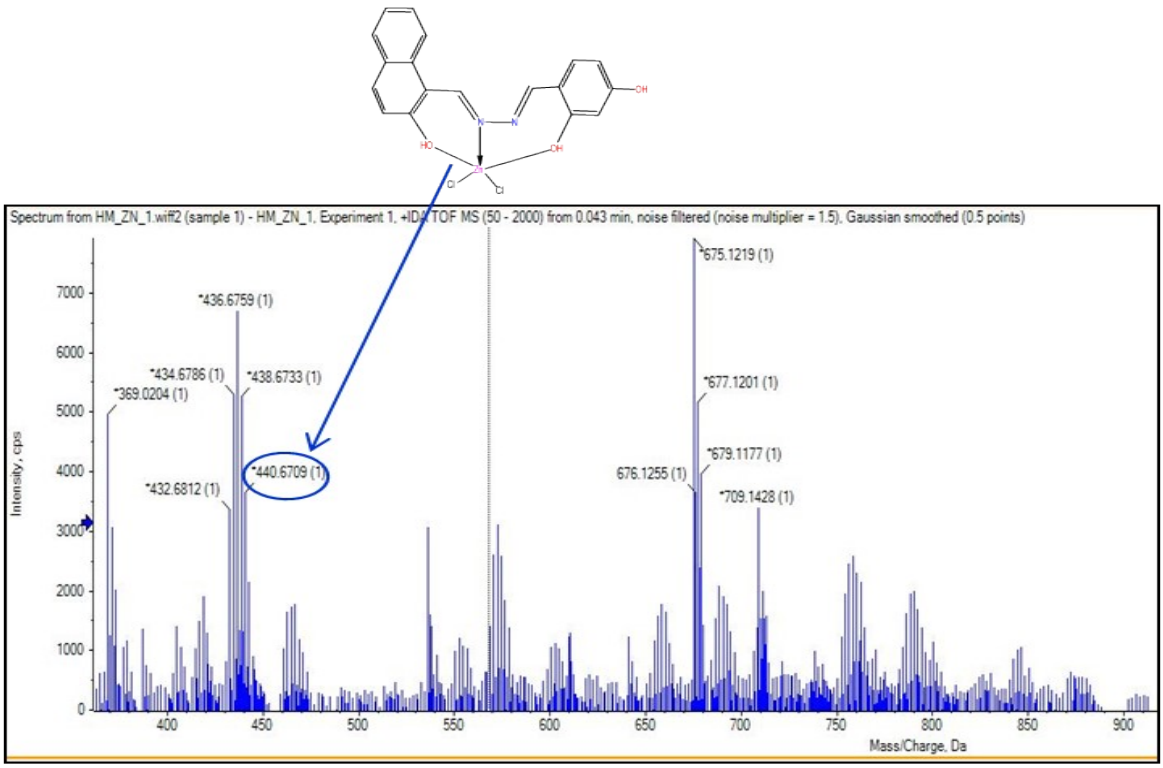

Fig. S19 Mass spectrum of **HMN**-Zn^{2+} complex

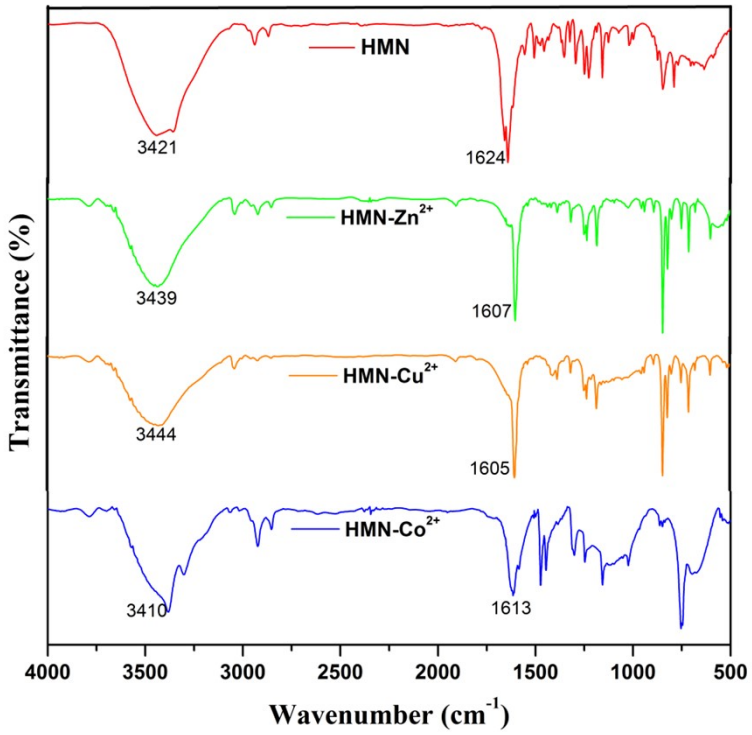

Fig. S20 IR spectrum of **HMN**, **HMN**-Zn^{2+}, **HMN**-Cu^{2+} and **HMN**-Co^{2+} complexes

Table S4 Comparison of experimental and theoretical vibrational frequencies of **HMN** and **HMN**-Zn^{2+}

Band assignments	Theoretical values (cm^{-1})	Intensity (calculated)	Experimental values (cm^{-1})
HMN			
ν (O-H)	3527	100.4	3421
ν (HC=N)	1622	124.5	1624
HMN-Zn^{2+}			
ν (O-H)	3350	445.0	3439
ν (HC=N)	1616	267.7	1607

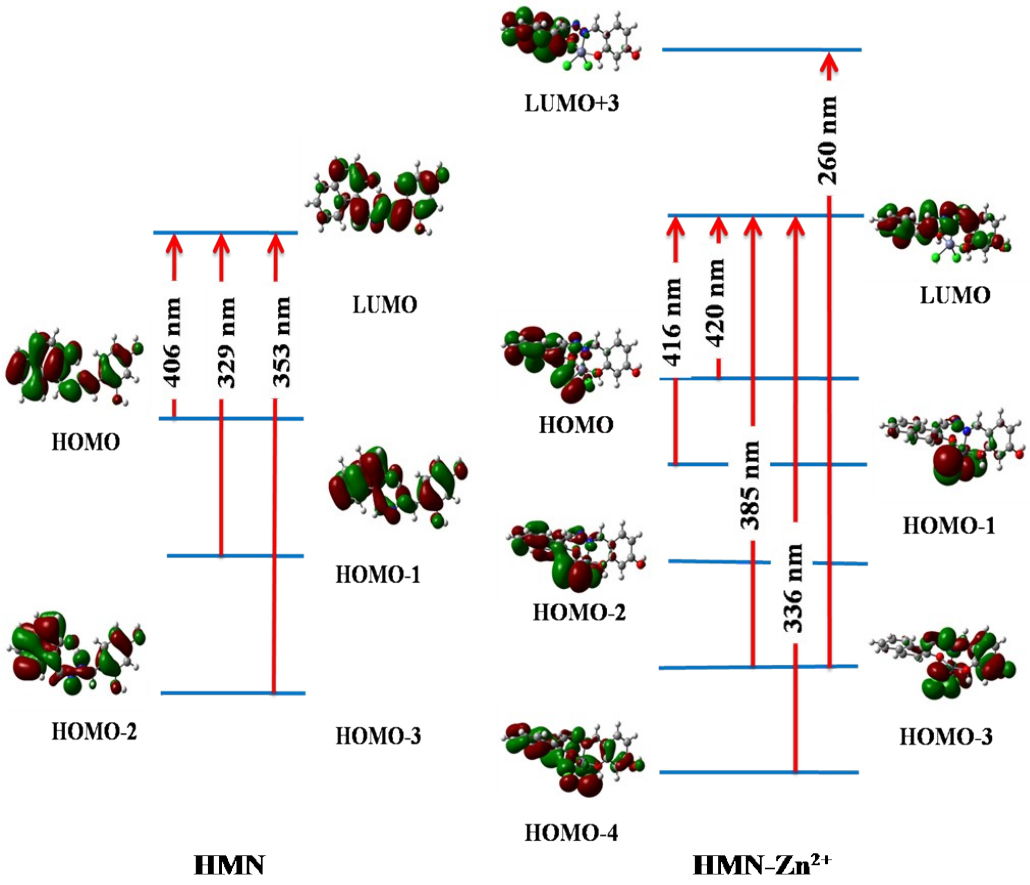

Fig. S21 Diagram displaying electronic transitions associated with **HMN** and **HMN**-Zn^{2+} (orbital contour value = 0.02)

Table S5 TD-DFT calculations for UV–visible transitions in **HMN** and **HMN**-Zn^{2+} complex with their assignments

Transition	Percent (%)	Wavelength (calc.)(nm)	Transition Character	Oscillator Strength	Wavelength (exp.)(nm)
		HMN			
H → L	70%	406	π → π*	0.330	392
H-1 → L	57%	329	π → π*	0.176	340
H-2 → L	26%		π → π*		
		HMN-Zn^{2+}			
H-1 → L	54%	416	MLCT	0.051	415
H → L	42%		π → π*		
H-2 → L	13%		π → π*		
H-3 → L	60%	385	π → π*	0.053	400
H → L	16%		π → π*		
H-4 → L	52%	336	π → π*	0.076	350
H-5 → L	30%				
H-6 → L	30%				
H → L+3	11%				

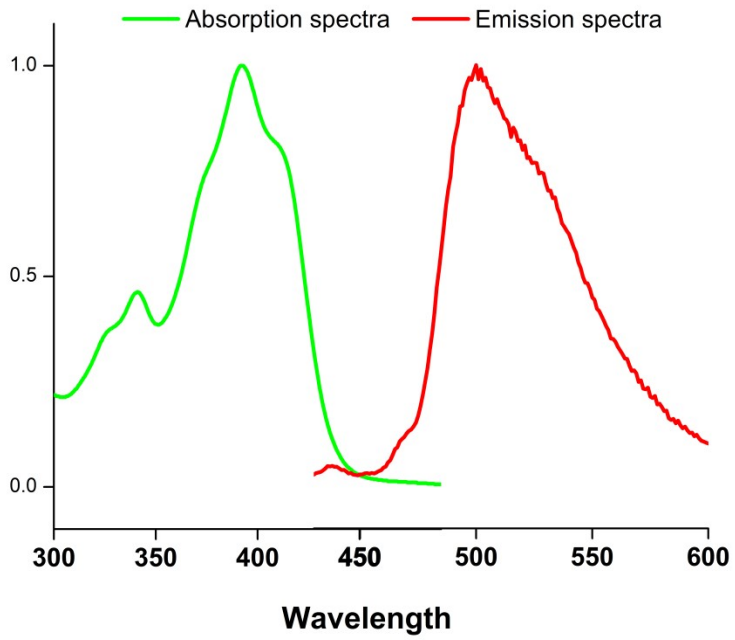

Fig. S22 Normalized absorption and emission spectra of **HMN**

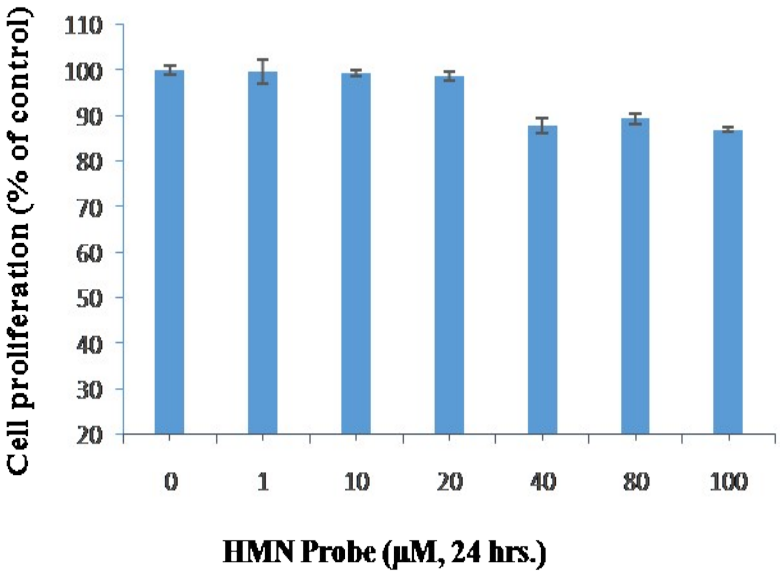

Fig. S23 The viability of cells examination by MTT assay after treatment of SiHa cells with indicated concentrations of **HMN** for 24 hrs at neutral pH

Table S6 Comparison of **HMN** with past reported probes

S. N.	Analytes	Binding constant (K_b) M^{-1}	Detection limit (LOD) M	Applications	Reference
1.	Cu^{2+}, Zn^{2+}	Cu^{2+}:2.1 × 10^7 Zn^{2+}:7.8 × 10^6	Cu^{2+}:1.4 × 10^{-7} Zn^{2+}: 7.2 × 10^{-8}	Bioimaging	8
2.	Zn^{2+}, OH^-	Zn^{2+}: 6.0 ×10^6	Zn^{2+} : 5.6 ×10^{-8}	Bioimaging	9
3.	Cu^{2+}	N/A	N/A	Real sample	10
4.	Zn^{2+}	N/A	Zn^{2+}: 1.1 × 10^{-7}	N/A	11
5.	Al^{3+}, Zn^{2+}	Al^{3+} :1.3 × 10^6 Zn^{2+} : 7.9 ×10^4	Al^{3+} : 8.3×10^{-8} Zn^{2+} : 1.2×10^{-7}	Bioimaging	12
6.	Mg^{2+}, Zn^{2+}	Mg^{2+} : 6.5×10^4 Zn^{2+} : 5.0×10^4	Mg^{2+}: 2.9×10^{-8} Zn^{2+} : 3.0×10^{-7}	Bioimaging, Real sample	13
7.	Al^{3+}, Zn^{2+}	Al^{3+}: 2.4 ×10^4 , 7.9 ×10^4 Zn^{2+} : 1.9 ×10^4 , 1.2 ×10^8	Al^{3+}: 5.9×10^{-6}, 5.7×10^{-6} Zn^{2+}: 3.3×10^{-6}, 5.2×10^{-6}	Bioimaging	14
8.	Co^{2+}, Cu^{2+}, Zn^{2+}	Co^{2+}: 2.057×10^5 Cu^{2+} : 5.385×10^4 Zn^{2+} : 8.09×10^4	Co^{2+} : 3.372×10^{-8} Cu^{2+} : 3.432×10^{-8} Zn^{2+} : 3.70×10^{-8}	Bioimaging, pH sensing, viscosity monitoring in apoptotic cells, mitotracking	This work

References

1. H.A. Benesi and J.H. Hildebrand, *J. Am. Chem. Soc.,* 1949, **71**, 2703–2707.
2. G.L. Long and J. D. Winefordner, *Anal. Chem.,* 1983, **55**, 712A–724A.
3. A.D. Becke, *J Chem Phys.,* 1993, **98**, 5648-5652.
4. G.M. Sheldrick, SHELXTL NT Version 5.1. Program for solution and refinement of crystal structures; University of Göttingen: Germany: 1997.
5. A. Parkin, G. Barr, W. Dong, C.J. Gilmore, D. Jayatilaka, J.J. McKinnon, M.A. Spackman and C.C. Wilson, *Cryst Eng Comm*, 2007**, 9***,* 648-652.
6. S.K. Wolff, D.J. Grimwood, J.J. McKinnon, M.J. Turner, D. Jayatilaka and M.A. Spackman, 2012. Crystal explorer.
7. P. Yadav, A.K. Singh, C. Upadhyay, and V.P. Singh, *Dyes Pigm.,* 2019**, 160**, 731-739.
8. X. He, Q. Xie, J. Fan, C. Xu, W. Xu, Y. Li, F. Ding, H. Deng, H. Chen, and J. Shen, *Dyes Pigm.*, 2020, **177**, 108255.
9. X. He, F. Ding, X. Sun, Y. Zheng, W. Xu, L. Ye, H. Chen and Shen, J. *Inorg. Chem.*, 2021, **60**, 5563-5572.
10. H. Qin, J. Huang, H. Liang and J. Li, *ACS Appl. Mater. Interfaces,* 2021, **13**, 5668−5677.
11. M. Shyamal, P. Mazumdar, S. Maity, S. Samanta, G. P. Sahoo and A. Misra, *ACS Sens.*, 2016**, 1**,739-747.
12. H. Liu, T. Liu, J. Li, Y. Zhang, J. Li, J. Song, J. Qu and W. Y. Wong, *J. Mater. Chem. B*, 2018**, 6**, 5435-5442.
13. Y. Wang, Z. G. Wang, X. Q. Song, Q. Chen, H. Tian, C. Z. Xie, Q. Z. Li and J. Y. Xu, *Analyst*, 2019**, 144**, 4024-4032.
14. W. Cao, X. J. Zheng, J. P. Sun, W. T. Wong, D. C. Fang, J. X. Zhang and L. P. Jin, *Inorg. Chem.*, **2014,** *53,* 3012-3021.